

DPD Parameters Estimation for Simultaneously Simulating Water-Oil Interfaces and Aqueous Non-Ionic Surfactants

Abeer Khedr and Alberto Striolo*

Chemical Engineering Department, University College London, United Kingdom

ABSTRACT

The outcome of a coarse-grained simulation within the Dissipative Particle Dynamics framework strongly depends on the choice of the repulsive parameter between different species. Different methodologies have been used in the literature to determine these parameters towards reproducing selected experimental system properties. In this work, a systematic investigation on possible procedures for estimating the simulation parameters is conducted. We compare methods based on the Hildebrand and the Hansen solubility parameter theories, mapped into the Flory-Huggins model. We find that using the Hansen solubility parameters it is possible to achieve a high degree of coarse graining, with parameters that yield realistic values for the interfacial tension. The procedure was first applied to the water/benzene system, and then validated for water/n-octane, water/1,1-dichloroethane, water/methyl cyclohexane, and water/isobutyl acetate. In all these cases, the experimental interfacial tension could be reproduced by adjusting a single correction factor. In the case of the water-benzene system, the Dissipative Particle Dynamics parameters derived using our approach were able to simultaneously describe both the interfacial tension and micellar properties of aqueous non-ionic surfactants representative of the octyl polyethylene oxide $C_8H_{17}O(C_2H_4O)_mH$ family. We show how the parameters can be used, within the Dissipative Particle Dynamics framework, to simulate the water/oil interface in presence of surfactants at varying concentrations. The results show, as expected, that as the surfactant concentration increases, the interfacial tension decreases and micelles form in bulk water.

Keywords: Interfacial tension, aggregation number, critical micelle concentration.

* Author to whom correspondence should be addressed: a.striolo@ucl.ac.uk

1. INTRODUCTION

Molecular simulations are widely used to provide molecular-level information to complement experimental data. Striolo and Grady¹ recently reviewed, for example, how experiments and simulations have been synergistically combined to investigate the adsorption of surfactants on a variety of substrates. While electronic-structure calculations are useful, e.g., in catalysis, and atomistic simulations reveal details such as the orientation of solvent molecules near surfaces, coarse-grained simulations can be implemented to investigate the emergent properties of complex fluids, e.g., surfactants²⁻⁴ and emulsions.⁵⁻⁷ Coarse-grained simulations allow us to sample length and time scales that approach experimental values, but at the expense of atomic-level descriptions of the phenomena. Among other coarse-grained approaches, the Dissipative Particle Dynamics (DPD) formalism is attracting significant attention.^{8,9} In such technique the particles (beads) represent group of molecules rather than atoms, and they interact with each other via soft potentials. DPD was introduced by Hoogerbrugge and Koelman,⁸ and modified later on.⁹⁻¹¹ Compared to other coarse-graining techniques based on ‘soft’ effective interaction potentials,¹² the simple soft DPD potential allows practitioners to use relatively long time steps, while providing a correspondence between DPD interaction parameters and thermodynamic properties (e.g., solubility parameters, as discussed below) without invoking complicated calculations.⁹

One of the most important parameters that can be tuned within a DPD simulation is the one describing repulsions between DPD beads. For pure fluids, this parameter is referred to as the ‘self-repulsion parameter’. Building on results for the compressibility of water, Groot and Warren⁹ related the self-repulsion parameter to the density within the simulation box and to the degree of coarse graining, as shown in Eq. (1):^{9,13,14}

$$a_{ii} = k_B T \frac{\kappa^{-1} N_m - 1}{2\alpha \rho_{\text{DPD}}} \quad (1)$$

In this equation a_{ii} is the repulsion parameter between same beads, k_B is the Boltzmann constant, T is the temperature of the system, κ^{-1} is the compressibility of water (equals to 15.9836 at 300 K), N_m is the degree of coarse-graining, ρ_{DPD} is the density inside the simulation box, and the coefficient α is estimated to be equal to 0.101 ± 0.001 .

When different fluids are simulated, one could tune the repulsive parameter between different beads to reproduce selected experimental properties or to match results obtained from atomistic simulations.¹⁵⁻¹⁷ Alternatively, one could define the repulsive DPD parameter ‘a priori’, starting from the thermodynamic properties of the pure components. For example,

Groot and Warren⁹ showed how to extract the DPD repulsive parameter from the χ_{ij} parameter of the Flory-Huggins model via the Eq. (2):

$$a_{ij} = (a_{ii} + 3.27 \chi_{ij}) \frac{k_B T}{r_c} \quad \text{at } \rho_{\text{DPD}} = 3 \quad (2)$$

In Eq. (2), a_{ij} is the repulsion parameter between different beads, χ_{ij} is the Flory-Huggins parameter between component i and j . The parameter a_{ij} is expressed in units of $k_B T/r_c$, where r_c is the cut-off distance, which defines the range of interaction between two beads. Maiti et al.¹⁴ showed that increasing the repulsion parameter to match relatively high degree of coarse-graining could yield a deviation from the experimental values of the interfacial tension. Instead of using parameters as calculated from Eq. (1), a reduced value of a_{ij} is often used in Eq. (2) to reproduce experimental interfacial tension data.¹⁸

The χ_{ij} parameter can be estimated experimentally, as well as via other approaches. Oviedo-Roa et al.,¹⁹ for example, reproduced the critical micelle concentration of dodecyl-trimethyl ammonium chloride when the Flory-Huggins χ_{ij} parameter between different entities was estimated using the infinite dilution activity coefficients as produced from quantum-atomistic simulations. On the other hand, according to the regular solution theory, the χ_{ij} parameter could be related to the solubility parameters of different species:^{20, 21}

$$\chi_{ij}(T) = \frac{V_i}{RT} (\delta_i(T) - \delta_j(T))^2 \quad (3)$$

In Eq. (3), $\delta_i(T)$ and $\delta_j(T)$ are the solubility parameters of component i and j , V_i is the molar volume of component i (in this notation, coefficient i represents the solvent, and j the solute), and R is the gas constant. It is worth noting that when DPD simulations are employed, it is common practice to use the volume of one bead as partial molar volume in Eq. (3).^{6, 14, 18}

Lindvig et al.²² discussed how the χ_{ij} parameter can be obtained from Hansen solubility parameters. The model proposed yielded a good prediction of the solubility of different polymers in a large group of solvents. The Hansen solubility parameters for component i results from contributions due to dispersion interactions ($\delta_{i,d}$), dipolar interactions ($\delta_{i,p}$), as well as hydrogen bonds effects ($\delta_{i,hb}$), all related to the Hildebrand solubility parameter δ_i according to:

$$\delta_i^2 = \delta_{i,d}^2 + \delta_{i,p}^2 + \delta_{i,hb}^2 \quad (4)$$

In the Hansen theory, the solubility parameters provide an accurate description of polar systems.²⁰ Lindvig and co-workers proposed to extract χ_{ij} from Hansen solubility parameters, using Eq. (5):

$$\chi_{ij} = \alpha \frac{V_i}{RT} \left((\delta_{i,d} - \delta_{j,d})^2 + 0.25(\delta_{i,p} - \delta_{j,p})^2 + 0.25(\delta_{i,hb} - \delta_{j,hb})^2 \right) \quad (5)$$

In Eq. (5) α is a correction factor. These Authors showed that changing this correction factor allows them to provide a good prediction of the thermodynamic property and solubility of four polymers [poly (butyl methacrylate), poly (methyl methacrylate), poly (ethyl methacrylate), and poly (vinyl acetate)] in various solvents (polar, non-polar, and hydrogen-bonding ones), and suggested a value of 0.6 as optimum for their systems.

In this work, we seek a procedure to determine the DPD repulsive parameters for a water/oil system in the presence of surfactants. The model parameters are validated by simultaneously representing the water/oil interfacial tension and the properties of the aqueous surfactant system. We screen parameters estimated using different solubility theories first, and then we carry on our simulations to identify the micellar properties in water. Finally, we simulate a water/oil system in presence of surfactants, proving that the simulations show a good representation of such a system. The study is conducted for a system composed of water/benzene containing a family of non-ionic polyethylene oxide surfactants. The reliability of the approach is then extended to a few water/organic liquid binary systems.

The remainder of this paper is organised as follows: In Section 2 we present the computational details. In Section 3, we validate the force-fields by comparing the simulations results obtained when the DPD parameters derived from different methodologies are implemented. In this section, we first consider the water/benzene system as a test case, and then we apply the procedure to a few other binary fluid systems. In section 4, we provide a detailed characterization of non-ionic surfactant aggregates in aqueous systems. Finally, in section 5 we discuss the results of the simulations for the water/benzene system in the presence of surfactants. We then briefly conclude summarizing our main findings.

2. Simulation Models and Algorithms

2.1. Dissipative Particle Dynamics

DPD is a class of coarse-grained simulations that was introduced by Hoogerbrugge and Koelman in 1992.⁸ In DPD, the total force acting on particle i (\mathbf{F}_i) is a summation of four

types of pair interactions: conservative $\mathbf{f}^C(\mathbf{r}_{ij})$, dissipative $\mathbf{f}^D(\mathbf{r}_{ij}, \mathbf{v}_{ij})$, random $\mathbf{f}^R(\mathbf{r}_{ij})$, and bonding $\mathbf{f}^S(\mathbf{r}_{ij})$, as shown in the following equations: ^{9, 23}

$$\mathbf{F}_i = \sum_{j \neq i} [\mathbf{f}^C(\mathbf{r}_{ij}) + \mathbf{f}^D(\mathbf{r}_{ij}, \mathbf{v}_{ij}) + \mathbf{f}^R(\mathbf{r}_{ij}) + \mathbf{f}^S(\mathbf{r}_{ij})] \quad (6)$$

$$\mathbf{f}^C(\mathbf{r}_{ij}) = \begin{cases} a_{ij} (1 - r_{ij}/r_c) \hat{\mathbf{r}}_{ij} & r_{ij} < r_c \\ 0 & r_{ij} \geq r_c \end{cases} \quad (7)$$

$$\mathbf{f}^D(\mathbf{r}_{ij}, \mathbf{v}_{ij}) = -\gamma \omega^D(r_{ij}) (\hat{\mathbf{r}}_{ij} \cdot \mathbf{v}_{ij}) \hat{\mathbf{r}}_{ij} \quad (8)$$

$$\mathbf{f}^R(\mathbf{r}_{ij}) = \sigma \omega^R(r_{ij}) \xi_{ij} \Delta t^{-1/2} \hat{\mathbf{r}}_{ij} \quad (9)$$

$$\mathbf{f}^S(\mathbf{r}_{ij}) = -k_s (r_{ij} - r_0) \hat{\mathbf{r}}_{ij} \quad (10)$$

The pair DPD interaction parameter a_{ij} determines the strength of the conservative forces, and describes the interactions between particles i and j . The vectors \mathbf{r}_{ij} and \mathbf{v}_{ij} are the distance ($\mathbf{r}_{ij} = \mathbf{r}_i - \mathbf{r}_j$) and the relative velocity ($\mathbf{v}_{ij} = \mathbf{v}_i - \mathbf{v}_j$) between particle i and j , respectively. $\hat{\mathbf{r}}_{ij}$ is the unit vector in the direction of \mathbf{r}_{ij} , and $r_{ij} = |\mathbf{r}_{ij}|$. r_c is the cut-off distance, which defines the effective interaction range, and represents the length scale in the DPD simulation. The variation of the friction coefficient and random force with distance are represented by $\omega^D(r_{ij})$ and $\omega^R(r_{ij})$, respectively. ξ_{ij} is a random number selected following a Gaussian distribution with zero mean and unit variance; γ is a coefficient controlling the strength of the frictional forces between the DPD beads; σ determines the magnitude of the random pair force between particles. To describe bonds, spring forces are introduced, which are described by k_s , the spring constant, and r_0 the equilibrium bond length. In order to conserve the Gibbs equilibrium conditions, $\omega^D(r_{ij})$ and $\omega^R(r_{ij})$, σ and γ are related by the following constraints:

$$\omega^D(r_{ij}) = [\omega^R(r_{ij})]^2 \quad (11)$$

$$\sigma^2 = 2k_B T \gamma \quad (12)$$

2.2. Coarse-Grained Models and Algorithms

All simulations presented here are conducted using the simulation package LAMMPS,²⁴ with the isothermal pair style DPD force fields. The random and dissipative parameters are set to $\sigma = 3$ and $\gamma = 4.5$.⁹ The time step $\Delta t = 0.04 \tau$ is used to integrate the equations of

motion. Simulations are performed in a rectangular box of dimensions $30 \times 30 \times 40 r_c^3$ ($L_x \times L_y \times L_z$). The simulations are intended to reproduce ambient conditions.

In the first instance, we simulate water, benzene, and surfactants. The degree of coarse graining of the water beads is chosen to be 5, which means that each DPD water bead represents 5 water molecules. Thus, the volume of one DPD bead (V_{bead}) equals $\sim 150 \text{ \AA}^3$. The density (ρ_{DPD}) in the simulation box is taken as 3, which means that the total number of beads is 108000 in all simulations. The cut-off distance (r_c) is taken as 1, and according to the relation $r_c = \sqrt[3]{\rho_{\text{DPD}} V_{\text{bead}}}$, r_c is equal to 7.66 \AA and the diameter of one bead equals $0.86 r_c$. Because this volume approximates that of one benzene molecule, in our representation one benzene molecule is represented by one DPD bead.

To validate the approach optimised for the water/benzene system, we also consider water/n-octane, water/1,1-dichloroethane, water/methyl cyclohexane, water/isobutyl acetate. For consistency, the degree of coarse graining was not changed compared to the water/benzene system.

We consider two non-ionic surfactants of the $C_8H_{17}O(C_2H_4O)_mH$ family. In the first one, the surfactant molecule is represented by three connected beads: one head represents one diethylene glycol group, and two tail beads represent three ethylene molecules, as shown in Figure 1. This surfactant is denoted as H1T2 in what follows. In the second surfactant, there are 3 head beads and 2 tail beads. This surfactant is denoted as H3T2. Consecutive beads in the surfactant molecule are connected with harmonic springs having an equilibrium bond length approximately equal to the bead diameter $r_0 = 0.9 r_c$, and spring constant $k_s = 100 k_B T / r_c^2$.²⁵

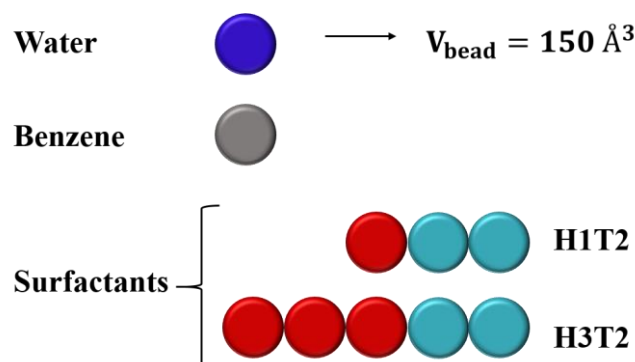


Figure 1. Schematic representation of the coarse-grained DPD beads representing the different components simulated in the systems considered in this work.

2.3. DPD Interaction Parameters

As briefly discussed above, in a DPD simulation box with density 3 and degree of coarse graining 5, the self-repulsion parameter (a_{ii}) should be 131.5 [see Eq. (1)]. However, the value 25 has often been used in the literature,^{14, 18} in an effort to reproduce experimental properties, as the estimation of a_{ij} depends on a_{ii} as discussed above [Eq. (2)].

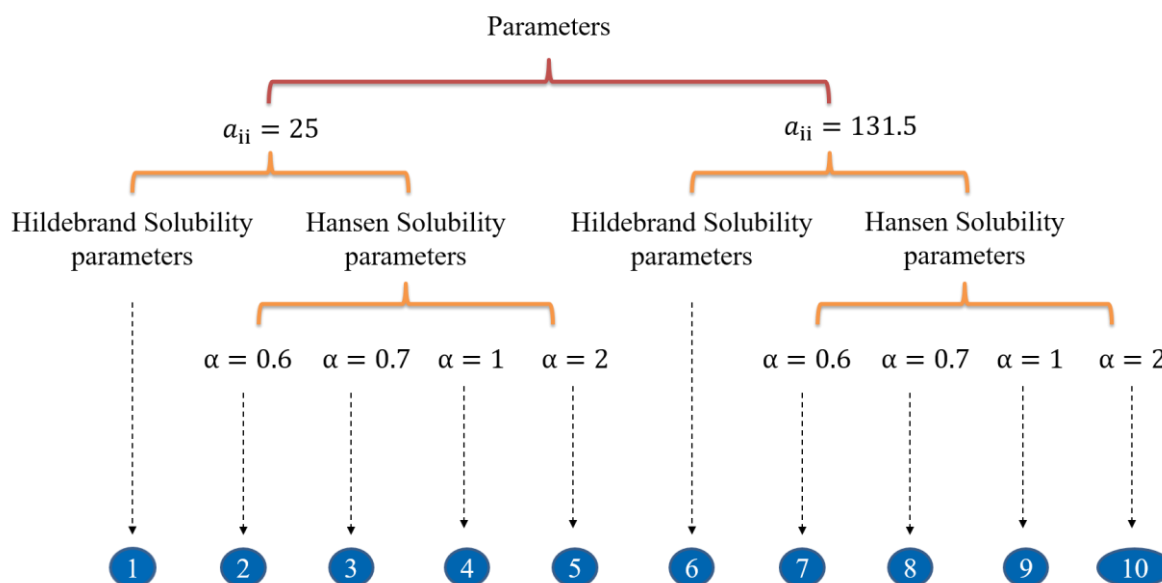


Figure 2. Different combination of parameters.

Using either $a_{ii} = 25$ or $a_{ii} = 131.5$, we considered different combinations of a_{ij} DPD parameters, as shown schematically in Figure 2. We systematically compared parameters derived from different solubility parameter theories, as well as the effect of the correction factor (α) in Eq. (5).²² Ultimately, we compare the ability of coarse-grained simulations to reproduce the water-benzene interfacial tension for the 10 combinations of parameters shown in Figure 2. To obtain the DPD parameters using different solution theories, we require the Hansen and the Hildebrand solubility parameters, which are listed in Table 1.²⁰ The values for $\delta_{\text{Hildebrand}}$ as listed in Table 1 are calculated from Eq. (4). All the parameters used for the 10 combinations of Figure 2 are listed in the supporting document (Table S1).

Table 1. Hansen and Hildebrand solubility parameters estimated at 25°C, in ($MPa^{1/2}$), and molar volume in $cc/mole$ for some of the compounds used in this study²⁰

Compound	δ_D	δ_P	δ_H	$\delta_{Hildebrand}$	V_{molar}
Water	15.5	16	42.3	47.81	18
Benzene	18.4	0	2	18.51	89.4
Diethylene glycol	16.6	12	20.7	29.12	94.9
Polyethylene	16	0.8	2.8	16.26	63

2.4. Computational details

The procedure is optimized for the water/benzene system. The interfacial tension is calculated by performing simulations for systems with equal number of beads of water and benzene (54000 beads each). Water and benzene phase separate. Water is at the bottom of the simulation box, benzene at the top, as shown in Figure 3. Note that the Z direction of the simulation box is perpendicular to the liquid-liquid interface. The interfacial tension between the two liquids is determined using the pressure tensors as shown in Eq. (13).¹⁴ The interfacial tension, γ_{DPD} , is averaged over the last 10^5 steps of a total 10^6 steps, after equilibrium has been reached.

$$\gamma_{DPD} = \frac{1}{2} \left\langle P_{zz} - \frac{(P_{xx} + P_{yy})}{2} \right\rangle L_z \quad (13)$$

To convert the calculated interfacial tension from the DPD units to mN/m, we multiply the simulated value by $k_B T / r_c^2$.¹⁴ It is worth noting that the factor $(\frac{1}{2})$ in Eq. (13) is due to the presence of two interfaces in our simulations, as shown in Figure 3.

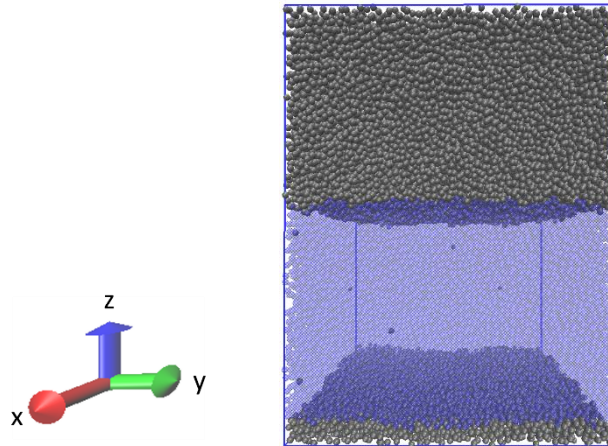


Figure 3. The water (transparent blue beads) - benzene (grey beads) system simulated here.

To quantify the properties of aqueous surfactants, simulations were conducted in bulk water at increasing surfactant volume fraction ϕ . As ϕ increases, surfactants might aggregate. To identify a cluster of surfactant molecules, we follow the approach proposed by Johnston and co-workers.²⁶ In this approach it is estimated that two surfactants belong to the same cluster when the distance between any of their hydrophobic tail beads is lower than $1 r_c$; note that this is the cut-off distance for the conservative interactions between DPD beads in our simulations. Once a micelle is identified, its properties are quantified as ensemble averages. Properties of interest include aggregation number, number of micelles in the simulation box, and the free surfactant volume fraction in the presence of micelles, which is used to estimate the critical micelle concentration (CMC). These properties are estimated after a total 2×10^6 simulation steps and averaged over 1.9×10^6 steps, considering the first 0.1×10^6 steps are the equilibrium time. Regarding the micellar shape, qualitative information is obtained by analysing snapshots taken at the end of 10^6 simulation steps.

The micellar properties depend on the cluster size cut-off, which means the aggregation number at which a cluster is considered as a micelle or as a surfactant aggregate (submicelles). Johnston et al.²⁶ reported the cluster size distribution for different surfactants. They used a minimum, or a gap in the cluster size distribution as the cluster size cut-off: clusters smaller than such cut-off were not considered micelles, clusters larger than such cut-off were considered as micelles. They found that this cut-off number could depend on the concentration of surfactant and the surfactant type. Building on this analysis, we calculated the cluster size distribution (based on aggregation number) of the simulated surfactants at different surfactant volume fractions with respect to the water beads (ϕ) as shown in the supporting document (Figure S1 and Figure S2). In agreement with the previous studies, the cut-off number was found to be dependent on the surfactant type and its volume fraction ϕ .

To calculate the critical micelle concentration (CMC) we implemented the approach proposed by Santos et al.,²⁷ who demonstrated that the CMC can be estimated by the constant value of the volume fraction free surfactant (ϕ_{oligomer}) in the accessible volume of aqueous phase (water beads in our case) when the total surfactant volume fraction in water (ϕ) increases. In Figure S3 and Figure S4 in supporting document, we report the number of micelles and ϕ_{oligomer} found in our simulation box as a function of simulation time for both surfactant molecules considered in this study. The results proved that 0.1×10^6 steps are enough to reach a dynamic equilibrium for our systems.

The correspondence between simulation time τ and real time can be estimated by comparing the experimental diffusion constant of water D_{water} (2.43×10^{-5} cm²/s) to the diffusion constant of the water beads in the DPD simulation, D_{sim} , as shown in Eq. (14).¹⁰ Following standard protocols, the simulated diffusion constant is calculated by the slope of the mean square displacement (MSD) of the water beads against time (in r_c^2/τ), as described by Eq. (15).

$$\tau = \frac{N_m D_{\text{sim}} r_c^2}{D_{\text{water}}} \quad (14)$$

$$D_{\text{sim}} = \frac{\text{MSD}}{6t} \quad (15)$$

Based on the procedure just summarized, we conclude that the time step in our simulations is equal to 15.2 ps and 5.45 ps in case of self-repulsion parameter equals 25 and 131.5 respectively. This decrease in the diffusion coefficient of the beads might be due to the fact that, as proved previously by Goicochea et al.,²⁵ increasing the self-repulsion parameter to match a high degree of coarse graining increases the excess pressure inside the simulation box according to:

$$p = \rho k_B T + \alpha \rho^2 \quad (\alpha = 0.101 \pm 0.001) \quad (16)$$

This increase in the excess pressure hinders the movement of the beads inside the simulation box, and by consequence, decreases the diffusion coefficient in DPD unit even if the density is constant. The dependency of the diffusion coefficient on the degree of coarse graining and the self-repulsion parameter were also studied by Pivkin et al.¹³ and they also found that increasing a_{ii} to match a high degree of coarse graining leads to a decrease in the diffusion coefficient.

3. Simulation Results – Model Validation

3.1. Interfacial tension

The experimental interfacial tension between water and benzene is 32.5 mN/m at 25 °C.²⁸ The water-benzene interfacial results as obtained from our simulations are summarized in Table 2. As expected based on literature observations,^{14, 18} in case of deriving the DPD parameters using the Hildebrand theory, realistic value for the interfacial tension is only produced at a self-repulsion parameter equals to 25. On the other hand, deriving the DPD parameters using the Hansen solubility theory yields interfacial tension values in reasonable

agreement with experiments when the self-repulsion parameter equals either 25 or 131.5, although for different values of the correction parameter α .

When the self-repulsive parameter is 25, the correction parameter α needs to be exceedingly high (2), while when the self-repulsive parameter is 131.5 (representing accurately the degree of coarse graining of 5 water molecules/bead), a reasonable value for α (0.7), yields a value for the simulated interfacial tension that is in good agreement with the experimental value. Presumably, adjusting α slightly above 0.7 could optimize the match between simulated and experimental interfacial tension when a_{ii} is 131.5. These results suggest that maintaining the original formalism and its relation to experimental observables (i.e., see Section 2.3) is critical for deriving sensible coarse-grained parameters.

The three sets of parameters that yield water/benzene interfacial tensions that are in reasonable agreement with experiments are identified as Model 1, Model 5 and Model 8 in Table 2. These are the sets of parameters that are used below to determine which one is also able to predict a realistic behaviour of surfactants in water.

Table 2. The simulated water/benzene interfacial tension using ten models. The underlined values are in reasonable agreement with experimental data

	IFT (mN/m)	a_{ii}	Solubility parameter theory
Model 1	<u>32</u> \pm 5	25	Hildebrand
Model 2	17.5 \pm 5	25	Hansen ($\alpha = 0.6$)
Model 3	20 \pm 5	25	Hansen ($\alpha = 0.7$)
Model 4	25.5 \pm 5	25	Hansen ($\alpha = 1$)
Model 5	<u>33</u> \pm 5	25	Hansen ($\alpha = 2$)
Model 6	61 \pm 9	131.5	Hildebrand
Model 7	26 \pm 8.5	131.5	Hansen ($\alpha = 0.6$)
Model 8	<u>30</u> \pm 8	131.5	Hansen ($\alpha = 0.7$)
Model 9	41.5 \pm 8.5	131.5	Hansen ($\alpha = 1$)
Model 10	65 \pm 8	131.5	Hansen ($\alpha = 2$)

3.2. Micelle formation

To identify the formation of micelles in aqueous systems we use Model 1, Model 5 and Model 8, as identified in Table 2. The simulations are conducted in bulk water at increasing

surfactant volume fraction φ . The results obtained for φ equal to 0.001, 0.003 and 0.05, in the form of simulation snapshots, are shown for the H1T2 surfactant in Figure 4. The results show that force-fields Model 1 and Model 5 yield surfactant aggregates already for surfactant volume fraction 0.001. Note that no free surfactants are observed for these parameterizations until φ equals 0.05. For the Model 8 parameterization, the results show that at low φ the surfactants are well dispersed in water. As the surfactant volume fraction increases, a micelle appears surrounded by free surfactant. This representation seems realistic, as it allows for the surfactants to exchange between the micelle and the free surfactants.

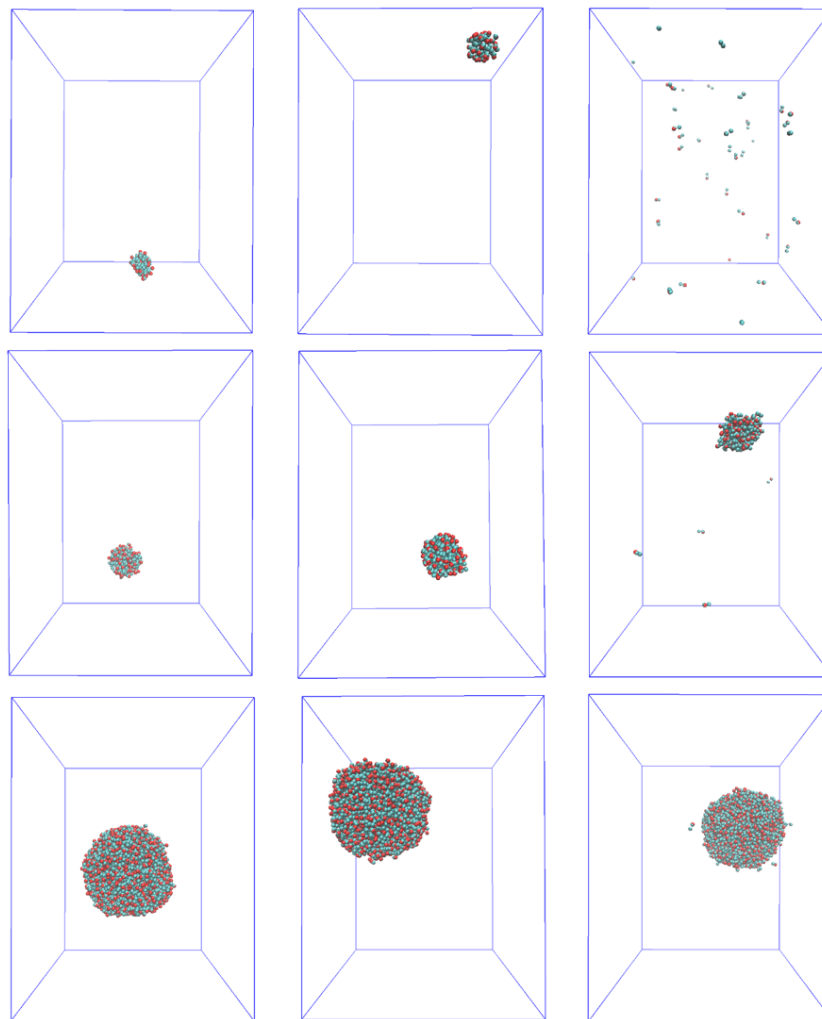


Figure 4. Aqueous surfactant H1T2 simulated at increasing volume fraction φ (top: 0.001; middle: 0.003; bottom: 0.05). From left to right, the snapshots represent results obtained for different force-fields: Model 1 (left); Model 5 (middle); Model 8 (right). The snapshots are obtained after 10^6 simulation steps.

Although the simulation results presented in Figure 4 suggest that Model 8 yields parameter that reproduce the properties of H1T2 surfactants in water, when we increased the surfactant volume fraction further, the single micelle grew, rather than multiple micelles appearing in equilibrium with free surfactant. The expected behaviour for surfactants instead is that as the surfactant volume fraction ϕ increases above the critical micelle concentrations, multiple micelles form.²⁶ Our simulations showed therefore evidence of phase separation between surfactant and water, rather than surfactant micelles formation in water.

To prevent phase separation, the repulsion parameter between water and the surfactant hydrophilic groups (head) was set to zero, following literature simulations for the STS,²⁹ as well as for the SDS surfactant in water.^{2, 4} We repeated the simulations discussed in Figure 4 for the three force-fields (Model 1, Model 5 and Model 8) but with the reduced repulsion between water and surfactant head-groups. The results are shown in Figure 5 for surfactant volume fraction ϕ equal to 0.001 and 0.003.

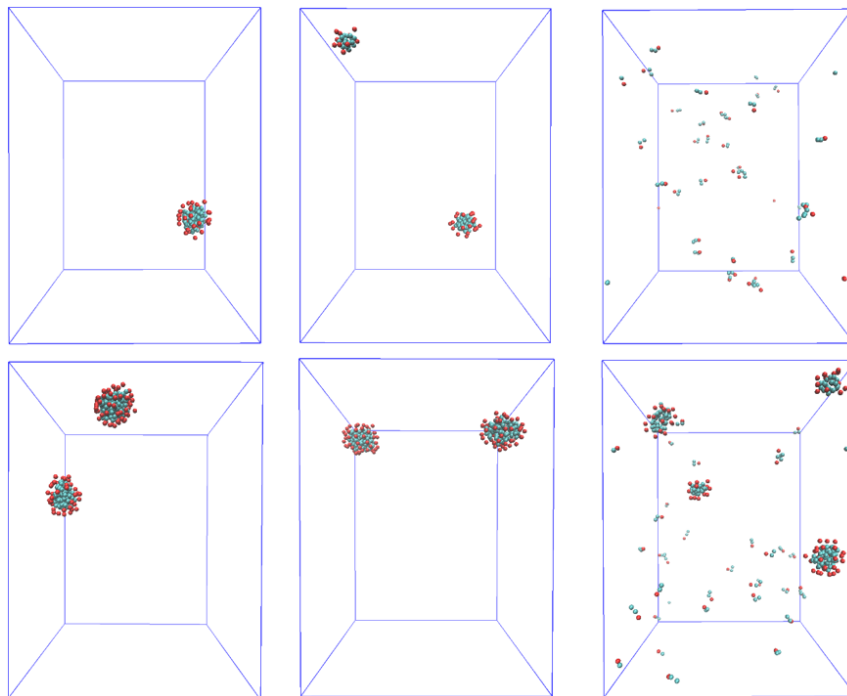


Figure 5. Aqueous surfactant H1T2 simulated at increasing volume fraction ϕ (top: 0.001; bottom: 0.003). From left to right, the snapshots represent results obtained for different force-fields: Model 1 (left); Model 5 (middle); Model 8 (right). As opposed to the results shown in Figure 4, the water-surfactant head-group repulsion parameter has been set to zero in these simulations. The snapshots are obtained after 10^6 simulation steps.

The results show that the surfactants yield multiple micelles for each of the force fields considered. However, the parameterization based on Model 1 and Model 5 does not allow for free surfactants in coexistence with the micelles. The Model force-field instead allows the description of multiple micelles in equilibrium with free surfactant. This force field is summarized in Table 3. Based on our results, DPD simulations based on such parameters predict realistic values for the water-benzene interfacial tension and describe realistic behaviour of aqueous HIT2 surfactants.

It is possible that Model 8 yields a realistic representation of the simulated system because the parameters are mapped from the proper coarse-graining degree and derived from the solubility parameters of the Hansen theory, which accounts for the contribution of dispersion, polar and hydrogen-bond effects.²⁰ Model 1 and Model 5 were derived from Hildebrand solubility parameters, based on the regular solution theory, which works best for nonpolar compounds where solvation and association effects are negligible.³⁰

Table 3. DPD force fields parameters, derived from Model 8 (see Table 2) that are able to both predict realistic water/benzene interfacial tension and realistic behaviour of aqueous HIT2 surfactants

	Water	Benzene	Head	Tail
Water	131.5	171.43	0	168.9
Benzene		131.5	142.07	132.01
Head			131.5	140.83
Tail				131.5

3.3. Other binary fluid systems

To assess the reliability of the approach described above to study the water/aromatic hydrocarbon interface, we consider here the interface between water and (a) one aliphatic hydrocarbon (n-octane), (b) one aliphatic halocarbon (1,1-dichloroethane), (c) one saturated cyclic compound (water/methyl cyclohexane), and (d) one ester (water/isobutyl acetate). These systems represent a variety of structural characteristics. For each binary system we compare the simulated interfacial tension against experimental data. As discussed above for Model 8, we impose $a_{ii} = 131.5$, and we calculate a_{ij} via Eq. (2) once χ_{ij} is estimated from Eq. (5) and the Hansen solubility parameter for the chosen compounds.

In Table 4, we list the number of beads that represents the different fluids according to their molar volume and the chosen degree of coarse-graining. We found that the correction factor varied from 0.4 to 1.4. This large variation reflects the fact that some interfaces require strong repulsion between different beads to yield high interfacial tension. In fact, our results show that the correction factor increases as the interfacial tension increases. A final note, for the 1,1-dichloroethane IFT with water, we compared to the available experimental values of 1,2-dichloroethane at 25°C.

Table 4. Calculated IFT (mN/m) of water/liquid systems from DPD simulations using Hansen solubility parameters and tuning the correction factor (α) in Eq. (5) to match the experimental data: ^{28, 31, 32}

	Model	Correction factor (α)	Water/liquid repulsion parameter	Experimental IFT at 25 °C	Simulated IFT
benzene	1 bead represents 1 molecule	0.7	171.43	32.5	30 ± 8
n-octane	2 beads represent 1 molecule	1.4	216.86	51.22	48 ± 11.5
1,1-dichloroethane	1 bead represents 1 molecule	0.8	170.03	28.4	29 ± 9
Methyl cyclohexane	3 beads represent 2 molecules	1	190.01	41.9	41.5 ± 13
Isobutyl acetate	3 beads represent 2 molecules	0.4	148.77	13.2	13.5 ± 12

4. Simulation Results – Aqueous Micellar Properties

4.1. Size distribution

Using the parameterisation discussed in Table 3, the surfactants H1T2 and H3T2 were simulated in water at different ϕ . The snapshots after 2×10^6 simulation steps are reported in Figure 6 and Figure 7, together with the enlargement of a representative micelle, respectively. The aggregation number distribution (cluster size distribution) is reported at $\phi = 0.18$ in Figure 8 (a) and (b) for H1T2 and H3T2 surfactants, respectively. Based on the cluster size distributions, the cluster cut-off is chosen as 10 for both surfactant types at this ϕ . This aggregation number shows a gap (Figure 8 (a)) and a minimum (Figure 8 (b)) in the cluster size distribution. All cluster size distributions as obtained for different volume fractions ϕ of both surfactant molecules are shown in the supporting document.

Once the cluster cut-off is identified, it is possible to classify clusters as micelles (their size is larger than the cut-off) or submicelles. The average number of micelles obtained at increasing surfactant volume fraction is shown in Figure 9 for both H1T2 and H3T2 surfactants. It is expected that the number of micelles in the systems increases linearly with ϕ . Instead, our results show a curvature, especially for the H3T2 surfactant. These results show that, as ϕ increases, the micelles increase in size. This behaviour is reported experimentally and, in some cases, leads to a micellar shape transformation (see the micellar shape section below).

In Figure 10, the mean aggregation number is calculated for the systems considered in Figure 9. Note that the submicelles are excluded from this analysis. At low surfactant volume fraction ϕ , a sudden increase in the aggregation number is observed due to the formation of the first micelles in the system. Instead of a constant aggregation number at high surfactant volume fraction, our results show a slow increase in the aggregation number. The results just discussed are consistent with the results shown in Figure 9. It should be noted that previous DPD simulations²⁶ also reported that the aggregation number is not constant after the formation of micelles. Instead, it depends on the surfactant volume fraction ϕ , and in general increases with ϕ following the law of mass action.

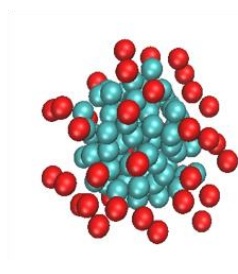
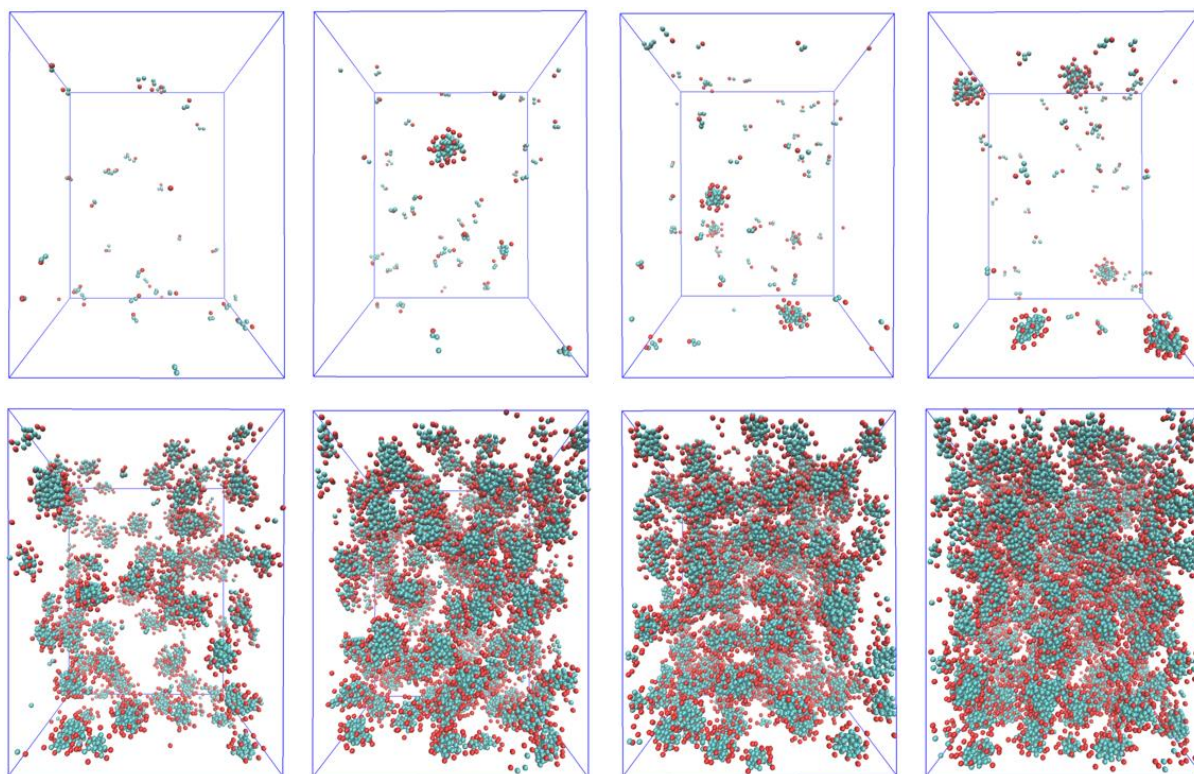


Figure 6. The aqueous H1T2 surfactant simulated at increasing volume fraction ϕ (left to right, top to bottom: 0.001, 0.002, 0.003, 0.005, 0.05, 0.11, 0.14, and 0.18). The snapshot at the bottom is an enlargement of a representative spherical micelle.

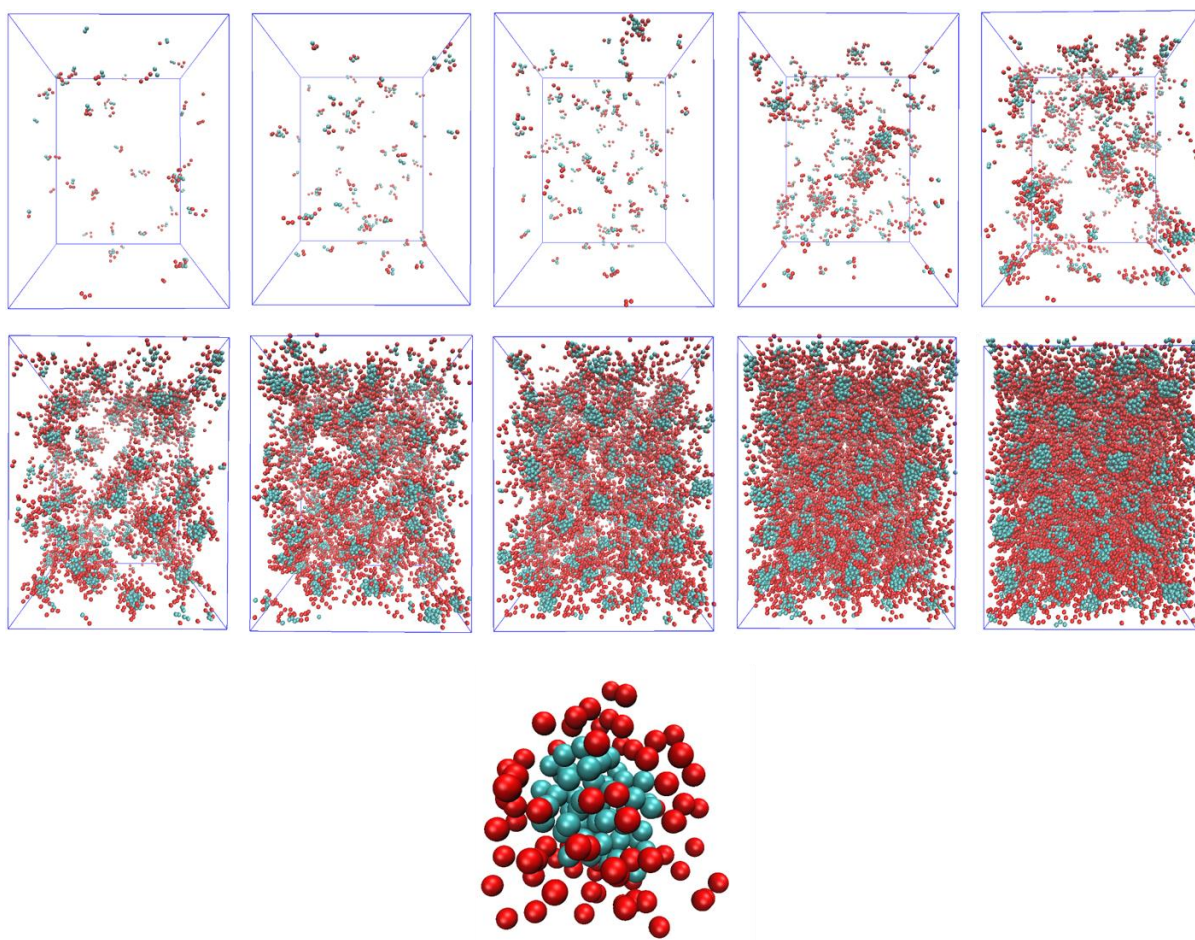


Figure 7. The aqueous H3T2 surfactant simulated at increasing volume fraction ϕ (left to right, top to bottom: 0.002, 0.003, 0.0042, 0.01, 0.02, 0.053, 0.087, 0.11, 0.176 and 0.2). The snapshot at the bottom is an enlargement of a representative spherical micelle.

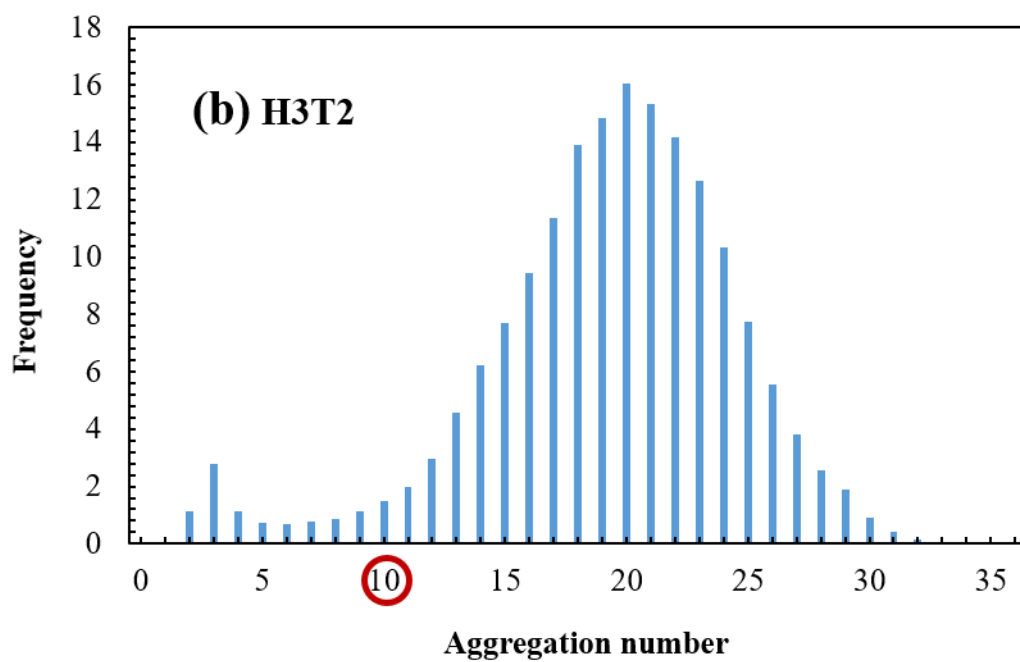
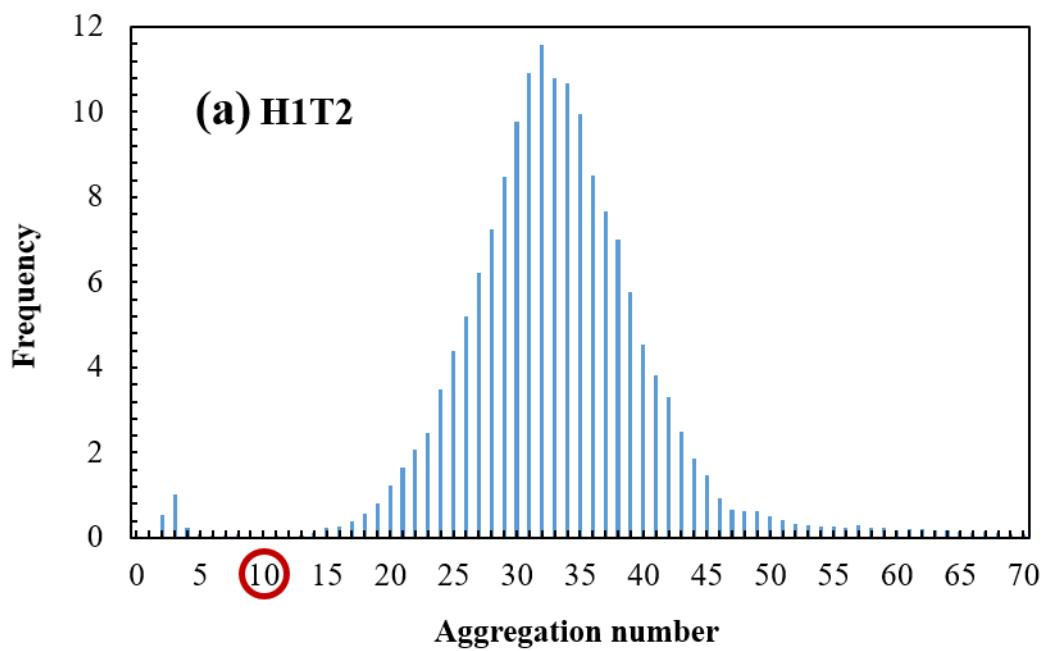


Figure 8. Cluster size distribution for aqueous (a) H1T2 and (b) H3T2 surfactants when ϕ equals 0.18. The red circle in the X-axis identifies the cluster cut-off.

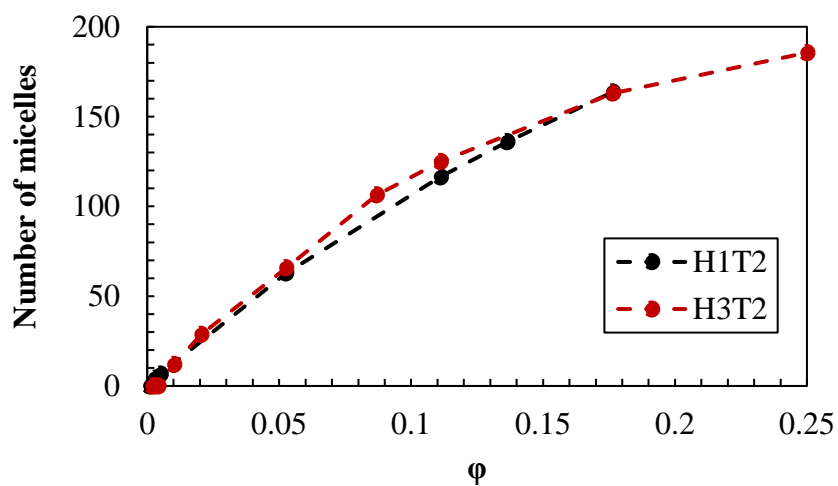


Figure 9. The increase in the number of micelles with increasing the surfactant volume fraction for both H1T2 and H3T2 surfactant molecules.

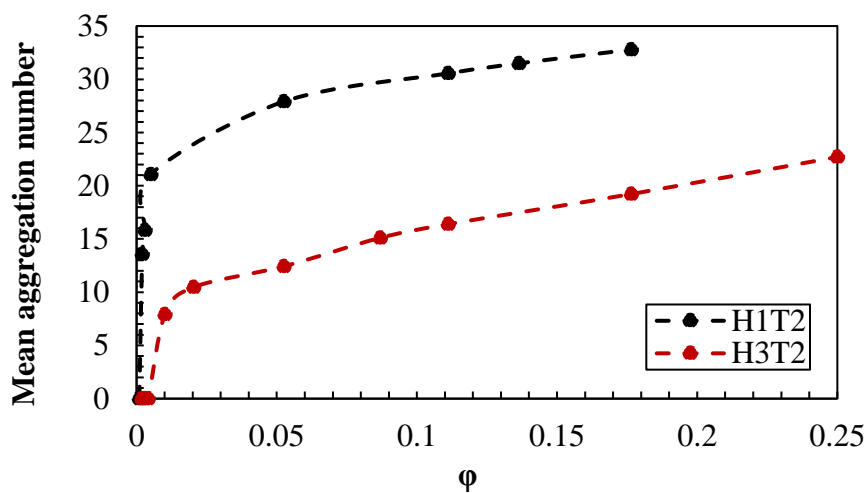


Figure 10. Mean aggregation number as a function of surfactant volume fraction for H1T2 and H3T2 surfactants.

4.2. Critical Micelle Concentration (CMC)

To estimate the critical micelle concentration (CMC) for H1T2 and H3T2 surfactants we calculate the volume fraction of the surfactant oligomers (ϕ_{oligomer}) as the surfactant volume fraction increases in our simulations. In Figure 11 we report the results: ϕ_{oligomer} increases as ϕ increases until the CMC is reached, after which ϕ_{oligomer} remains constant. This plateau is reached at $\phi_{\text{oligomer}} = 0.00125$, equivalent to 0.004624 ± 0.0004 mole/litre for H1T2, and at $\phi_{\text{oligomer}} = 0.006$, equivalent to 0.01402 ± 0.0017 mole/litre for H3T2. In the case of H3T2, It was found that at surfactant volume fraction 0.0042, just below the CMC, unstable micelle was found then it dissolved in the bulk water again. This concentration is not included in our calculations of the CMC or in the properties mentioned above.

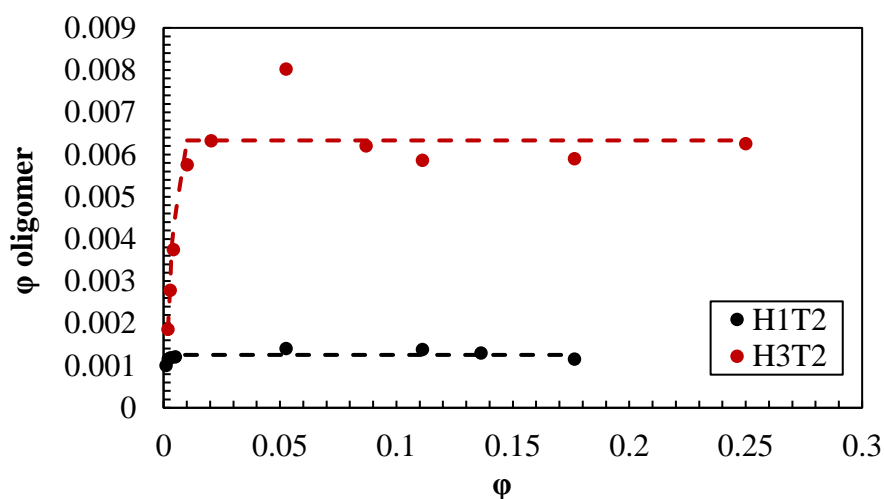


Figure 11. Volume fraction of the free surfactant (ϕ_{oligomer}) as a function of ϕ for aqueous H1T2 and H3T2 surfactants. The results are averaged over the last 1.9×10^6 steps of the total 2×10^6 steps for each simulation.

The CMC results are compared in Table 5 to experimental values reported for polyethylene oxide non-ionic surfactants.³³⁻³⁵ The simulated CMC for H1T2 is similar to the experimental one for octyl polyethylene oxide C_8E_1 (0.0049 mole/litre).^{33, 34} The simulated CMC increases as the length of the hydrophilic group increases (i.e., compare results for H1T2 to H3T2 surfactants). This is consistent with experiments, as the simulated CMC for H3T2 is similar to the experimental one for C_8E_9 (0.013 mole/litre).^{33, 35}

Table 5. CMC in mole/litre determined from simulations and reported from experiments

Simulation	Experiment
0.0046 ± 0.0004	0.0049
H1T2	C ₈ E ₁ (octyl glycol ether)
0.0140 ± 0.0017	0.013
H3T2	C ₈ E ₉ (nonaoxyethylene glycol monoether)

4.3. Micellar shape

It has been reported that micelles for some non-ionic polyethylene oxide surfactants transform from spherical to rod-like as the surfactant concentration increases.^{36, 37} For example, Nilsson et al.³⁸ reported that the size of C₁₂E₅ micelles increases and exhibit a shape transition from spherical to rod-like micelles with increasing surfactant concentration. Consistently with these experimental observations, at low surfactant volume fractions we observe spherical micelles with different aggregation numbers for both H1T2 and H3T2 simulated surfactants (Figure 6 and Figure 7). When the volume fraction of aqueous H1T2 is increased to $\phi = 0.43$, we observe micelles with ellipsoidal shape, as well as rod-like micelles. A similar shape transformation is observed for H3T2 in water when the volume fraction is increased to $\phi = 1$. Snapshots of these two simulations are shown in Figure 12 along with examples of micelles observed in both systems.

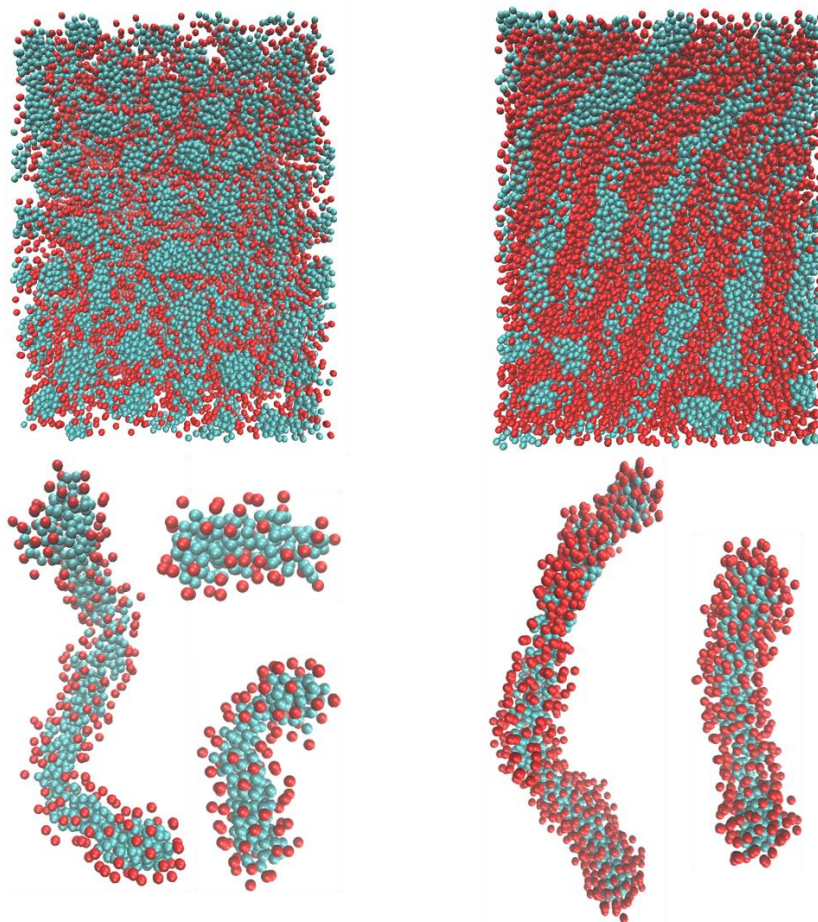


Figure 12. The ellipsoidal and rod-like micelles observed for H1T2 (left) and H3T2 (right) at ϕ 0.43 and 1, respectively, after 10^6 simulations steps.

5. Water/Benzene/Surfactant Systems

The parameterization of Table 3 is able to reproduce the water/benzene interfacial tension as well as several properties of aqueous micelles for both H1T2 and H3T2 surfactants. This parameterization is implemented here to simulate water/benzene interfaces in the presence of surfactants. We prepare a simulation box with an equal amount of beads representing water and benzene (number of beads of each constituent are listed in Table 6 for different simulations). As the simulation progresses, water and benzene phase separate. The Z direction of the simulation box is perpendicular to the water-benzene interface. When surfactants are present in the system, they are expected to accumulate at the water/benzene interfaces. Figure 13 (a) and (b) show representative simulation snapshots obtained when 300 surfactants (either H1T2 or H3T2) are introduced to water/benzene system.

Table 6. Number of water/benzene/surfactant beads in all simulations in Section 5

Molecules	H1T2			H3T2		
Water	53550	52500	52200	53250	522500	51000
Benzene	53550	52500	52200	53250	52250	51000
Surfactants (Head/Tail)	300/600	1000/2000	1200/2400	900/600	2100/1400	3600/2400

At these conditions, we find little, if any surfactant in the bulk phases. At these conditions, the water/benzene interfacial tension (30 mN/m) is reduced to 26.3 ± 9.6 and 26.6 ± 9.2 mN/m by 300 H1T2 and H3T2 surfactants, respectively. When the number of H1T2 and H3T2 surfactant molecules is increased to 1000 and 700, respectively, the interfacial tension is reduced to 17.4 ± 8.5 and 16.3 ± 10 mN/m, respectively. The correspondent snapshots are shown in Figure 13 (c) and (d). The surfactant concentrations were chosen, via trial and error, to achieve maximum interfacial saturation before surface deformation.

Increasing the surfactant concentration further to 1200 molecules, the water/benzene interfaces saturate, and micelles appeared in bulk water. At these conditions, oil beads were found inside the micelles, suggesting that the simulations are consistent with the formation of micro-emulsions. A schematic representation of these later simulations is shown in Figure 14 with snapshots of the micelles contain benzene beads in both surfactant molecules.

We conclude that the DPD parameterization of Table 3 yields properties of the water/benzene/H1T2 and water/benzene/H3T2 systems that are qualitatively consistent with experimental expectations.

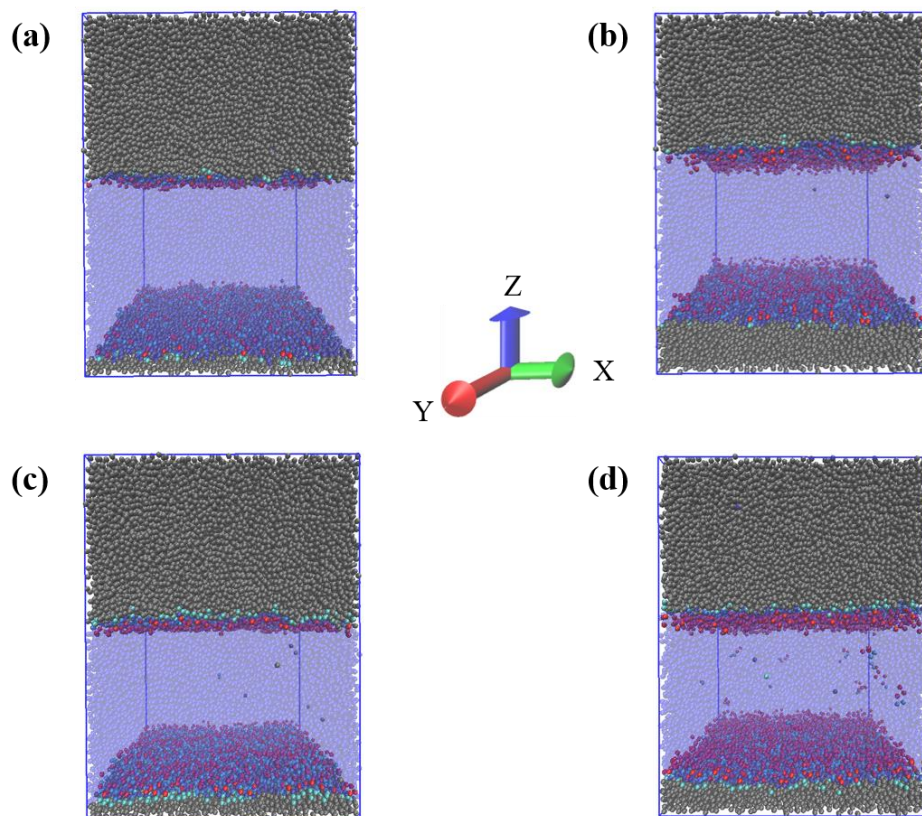


Figure 13. Representative snapshots for water/benzene/H1T2 (left) and water/benzene/H3T2 (right) systems containing 300 (a and b), 1000 H1T2 (c) and 700 H3T2 (d) surfactants.

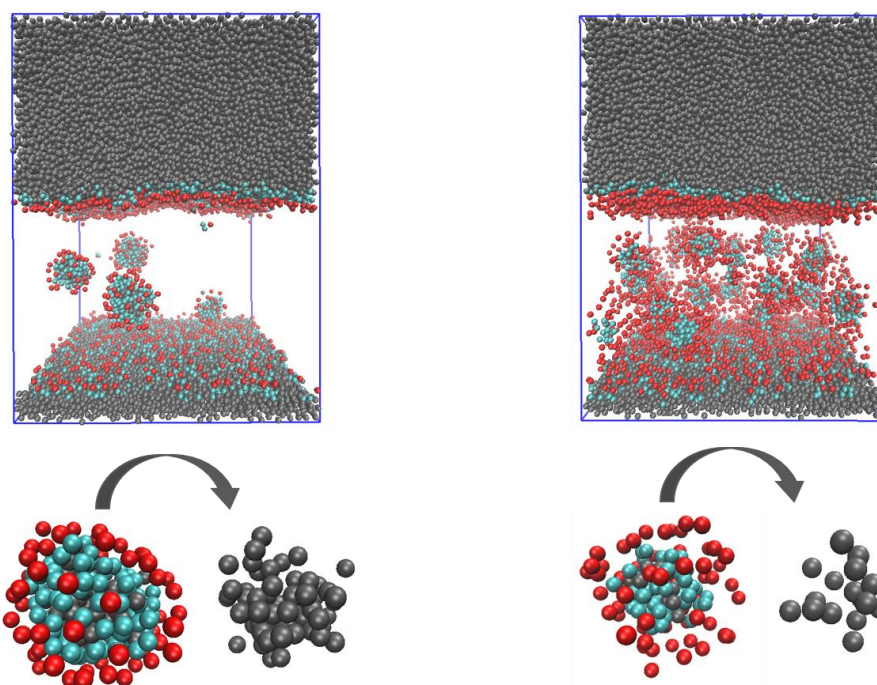


Figure 14. Snapshots of water/benzene system in presence of 1200 molecules of H1T2 (left) and H3T2 (right), with oil beads entrapped inside micelles found in each simulation (bottom).

Oil beads are shown in grey.

6. Conclusions

In this work, we implemented a systematic process for determining DPD parameters for simulating water/oil interfaces in the presence of non-ionic surfactants. The Hansen/Flory-Huggins theory proved its ability to provide parameters that reproduce experimental interfacial tension consistent with the degree of coarse graining selected for the simulations. The approach was optimised for the water/benzene system and validated for other binary liquid systems. Our results show that to reproduce the properties of aqueous micelles formed by non-ionic surfactants of the $C_8H_{17}O(C_2H_4O)_mH$ family, it is necessary to strongly reduce the repulsive parameters between water and surfactant head groups.

The resultant parameterization is able to simulate the expected behaviour of non-ionic surfactants in water and to predict their critical micelle concentration in good agreement with experiments, including the dependency of the CMC on the length of the surfactant head group and the shape transformation of micelles as the surfactant volume fraction increases. When the parameterization is implemented to simulate water/benzene/surfactant systems the results are in qualitative agreement with experiments. They show that the surfactants accumulate at the liquid/liquid interface reducing the interfacial tension; that the surfactants do not distribute significantly on either pure bulk phase until the interfaces are saturated by surfactants; and that when the surfactant amount increases further, the surfactants deform the interface and distribute preferentially in the aqueous phase where they form micelles containing oil beads.

Supporting Information

The repulsion parameters for DPD models; the cluster size distribution of H1T2 and H3T2 micelles at different surfactant volume fraction ϕ ; number of H1T2 and H3T2 micelles in water at different ϕ ; and ϕ_{oligomer} change with time for H1T2 and H3T2 in water at different ϕ . This material can be found free of charge on the ACS Publications website at DOI:

Acknowledgments

Generous allocations of computing time were provided by the University College London Research Computing Platforms Support (LEGION), and the National Energy Research Scientific Computing Center (NERSC) at Lawrence Berkeley National Laboratory. NERSC is supported by the DOE Office of Science under Contract DE-AC0205CH11231. The authors

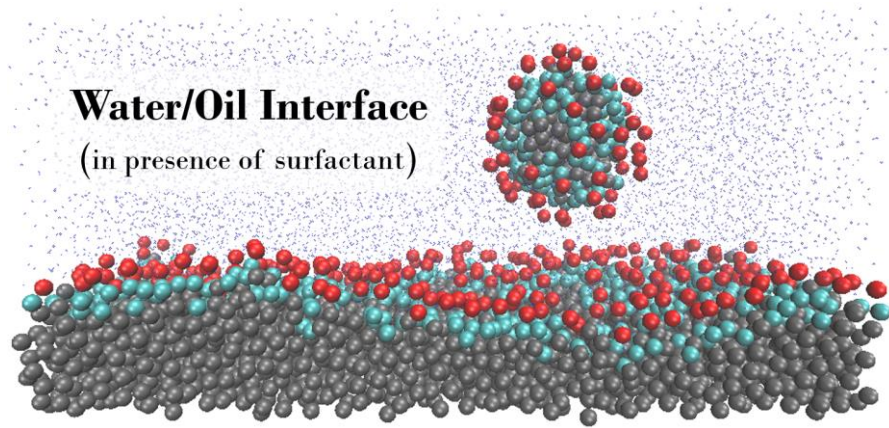
also acknowledge financial support from the Department of Chemical Engineering at the University College London.

References

- (1) Striolo, A.; Grady, B. P. Surfactant Assemblies on Selected Nanostructured Surfaces: Evidence, Driving Forces, and Applications. *Langmuir*. **2017**, *33*, 8099-8113.
- (2) Suttipong, M.; Grady, B. P.; Striolo, A. Self-Assembled Surfactants on Patterned Surfaces: Confinement and Cooperative Effects on Aggregate Morphology. *Phys. Chem. Chem. Phys.* **2014**, *16*, 16388-16398.
- (3) Suttipong, M.; Grady, B. P.; Striolo, A. Surfactant Aggregates Templated by Lateral Confinement. *J. Phys. Chem. B*. **2015**, *119*, 5467-5474.
- (4) Suttipong, M.; Grady, B. P.; Striolo, A. Surfactants Adsorption on Crossing Stripes and Steps. *Soft Matter*. **2017**, *13*, 862-874.
- (5) Alvarez, F.; Flores, E. A.; Castro, L. V.; Hernandez, J. G.; Lopez, A.; Vazquez, F. Dissipative Particle Dynamics (Dpd) Study of Crude Oil-Water Emulsions in the Presence of a Functionalized Co-Polymer. *Energy Fuels*. **2011**, *25*, 562-567.
- (6) Lin, S. L.; Xu, M. Y.; Yang, Z. R. Dissipative Particle Dynamics Study on the Mesostuctures of N-Octadecane/Water Emulsion with Alternating Styrene-Maleic Acid Copolymers as Emulsifier. *Soft Matter*. **2012**, *8*, 375-384.
- (7) Song, X. Y.; Shi, P.; Duan, M.; Fang, S. W.; Ma, Y. Z. Investigation of Demulsification Efficiency in Water-in-Crude Oil Emulsions Using Dissipative Particle Dynamics. *RSC Adv.* **2015**, *5*, 62971-62981.
- (8) Hoogerbrugge, P. J.; Koelman, J. M. V. A. Simulating Microscopic Hydrodynamic Phenomena with Dissipative Particle Dynamics. *EUROPHYS. LETT.* **1992**, *19*, 155.
- (9) Groot, R. D.; Warren, P. B. Dissipative Particle Dynamics: Bridging the Gap between Atomistic and Mesoscopic Simulation. *J. Chem. Phys.* **1997**, *107*, 4423-4435.
- (10) Groot, R. D.; Rabone, K. L. Mesoscopic Simulation of Cell Membrane Damage, Morphology Change and Rupture by Nonionic Surfactants. *Biophys. J.* **2001**, *81*, 725-736.
- (11) Espanol, P.; Warren, P. Statistical-Mechanics of Dissipative Particle Dynamics. *EUROPHYS. LETT.* **1995**, *30*, 191-196.
- (12) Forrest, B. M.; Suter, U. W. Accelerated Equilibration of Polymer Melts by Time-Coarse-Graining. *J. Chem. Phys.* **1995**, *102*, 7256-7266.

- (13) Pivkin, I. V.; Karniadakis, G. E. Coarse-Graining Limits in Open and Wall-Bounded Dissipative Particle Dynamics Systems. *J. Chem. Phys.* **2006**, *124*.
- (14) Maiti, A.; McGrother, S. Bead-Bead Interaction Parameters in Dissipative Particle Dynamics: Relation to Bead-Size, Solubility Parameter, and Surface Tension. *J. Chem. Phys.* **2004**, *120*, 1594-1601.
- (15) Fan, H.; Striolo, A. Mechanistic Study of Droplets Coalescence in Pickering Emulsions. *Soft Matter*. **2012**, *8*, 9533-9538.
- (16) Fan, H.; Striolo, A. Nanoparticle Effects on the Water-Oil Interfacial Tension. *Phys. Rev. E*. **2012**, *86*, 051610.
- (17) Luu, X.-C.; Yu, J.; Striolo, A. Nanoparticles Adsorbed at the Water/Oil Interface: Coverage and Composition Effects on Structure and Diffusion. *Langmuir*. **2013**, *29*, 7221-7228.
- (18) Shi, K. H.; Lian, C.; Bai, Z. S.; Zhao, S. L.; Liu, H. L. Dissipative Particle Dynamics Study of the Water/Benzene/Caprolactam System in the Absence or Presence of Non-Ionic Surfactants. *CHEM. ENG. SCI.* **2015**, *122*, 185-196.
- (19) Oviedo-Roa, R.; Martinez-Magadan, J. M.; Munoz-Colunga, A.; Gomez-Balderas, R.; Pons-Jimenez, M.; Zamudio-Rivera, L. S. Critical Micelle Concentration of an Ammonium Salt through Dpd Simulations Using Cosmo-Rs-Based Interaction Parameters. *AICHE J.* **2013**, *59*, 4413-4423.
- (20) Hansen, C. M. *Hansen Solubility Parameters: A User's Handbook*. 2nd ed.; CRC Press: Boca Raton, 2007.
- (21) Hildebrand, J. An Improvement in the Theory of Regular Solutions. *Proc. Natl. Acad. Sci. U.S.A.* **1979**, *76*, 6040-6041.
- (22) Lindvig, T.; Michelsen, M. L.; Kontogeorgis, G. M. A Flory-Huggins Model Based on the Hansen Solubility Parameters. *Fluid Ph. Equilibria*. **2002**, *203*, 247-260.
- (23) Frenkel, D.; Smit, B. *Understanding Molecular Simulation* 2nd ed.; Academic Press, Inc.: Orlando, Florida, 2002; Vol. 1, pp 465-476.
- (24) Plimpton, S. Fast Parallel Algorithms for Short-Range Molecular-Dynamics. *J. Comput. Phys.* **1995**, *117*, 1-19.
- (25) Goicochea, A. G.; Romero-Bastida, M.; Lopez-Rendon, R. Dependence of Thermodynamic Properties of Model Systems on Some Dissipative Particle Dynamics Parameters. *Mol. Phys.* **2007**, *105*, 2375-2381.

- (26) Johnston, M. A.; Swope, W. C.; Jordan, K. E.; Warren, P. B.; Noro, M. G.; Bray, D. J.; Anderson, R. L. Toward a Standard Protocol for Micelle Simulation. *J. Phys. Chem. B.* **2016**, *120*, 6337-6351.
- (27) Santos, A. P.; Panagiotopoulos, A. Z. Determination of the Critical Micelle Concentration in Simulations of Surfactant Systems. *J. Chem. Phys.* **2016**, *144*.
- (28) Albaz, M.; Bilgesu, A.; Tutkun, O. The Measurement of Interfacial Tension by Drop-Weight Method. *Commun. Fac. Sci. Univ. Ank. Ser. B.* **1988**, *34*, 103-112.
- (29) Kuo, M. Y.; Yang, H. C.; Hua, C. Y.; Chen, C. L.; Mao, S. Z.; Deng, F.; Wang, H. H.; Du, Y. R. Computer Simulation of Ionic and Nonionic Mixed Surfactants in Aqueous Solution. *Chemphyschem.* **2004**, *5*, 575-580.
- (30) Hildebrand, J. H.; Wood, S. E. The Derivation of Equations for Regular Solutions. *J. Chem. Phys.* **1933**, *1*, 817-822.
- (31) Freitas, A. A.; Quina, F. H.; Carroll, F. A. Estimation of Water– Organic Interfacial Tensions. A Linear Free Energy Relationship Analysis of Interfacial Adhesion. *J. Phys. Chem. B.* **1997**, *101*, 7488-7493.
- (32) Aveyard, R.; Haydon, D. A. Thermodynamic Properties of Aliphatic Hydrocarbon-Water Interfaces. *T Faraday Soc.* **1965**, *61*, 2255-&.
- (33) Huibers, P. D. T.; Lobanov, V. S.; Katritzky, A. R.; Shah, D. O.; Karelson, M. Prediction of Critical Micelle Concentration Using a Quantitative Structure-Property Relationship Approach .1. Nonionic Surfactants. *Langmuir.* **1996**, *12*, 1462-1470.
- (34) Shinoda, K.; Yamanaka, T.; Kinoshita, K. Surface Chemical Properties in Aqueous Solutions of Nonionic Surfactants - Octyl Glycol Ether, Alpha-Octyl Glyceryl Ether and Octyl Glucoside. *J. Phys. Chem.* **1959**, *63*, 648-650.
- (35) Corkill, J. M.; Goodman, J. F.; Harrold, S. P. Thermodynamics of Micellization of Non-Ionic Detergents. *Trans. Faraday Soc. .* **1964**, *60*, 202-&.
- (36) Rosevear, F. B. Liquid Crystals - Mesomorphic Phases of Surfactant Compositions. *J. Soc. Cosmetic Chemists.* **1968**, *19*, 581-594.
- (37) Mitchell, D. J.; Tiddy, G. J. T.; Waring, L.; Bostock, T.; Mcdonald, M. P. Phase-Behavior of Polyoxyethylene Surfactants with Water - Mesophase Structures and Partial Miscibility (Cloud Points). *J. Chem. Soc. Faraday Trans. I.* **1983**, *79*, 975-1000.
- (38) Nilsson, P. G.; Wennerstroem, H.; Lindman, B. Structure of Micellar Solutions of Nonionic Surfactants. Nuclear Magnetic Resonance Self-Diffusion and Proton Relaxation Studies of Poly (Ethylene Oxide) Alkyl Ethers. *J. Phys. Chem.* **1983**, *87*, 1377-1385.



TOC graphic